RSC Advances

PAPER

View Article Online
View Journal | View Issue

Check for updates

Cite this: *RSC Adv.*, 2024, **14**, 21292

A novel nanodrug for the sensitization of photothermal chemotherapy for breast cancer *in vitro*†

Ji Chuan Kong, * Feng Zhou, Liting Shi, Yihui Wei and Chunhong Wu*

Received 1st March 2024
Accepted 4th June 2024

DOI: 10.1039/d4ra01611d

rsc.li/rsc-advances

Owing to the complexity of tumor treatment, clinical tumor treatment has evolved from a single treatment mode to multiple combined treatment modes. Reducing the tolerance of tumors to heat and the toxicity of chemotherapy drugs to the body, as well as increasing the sensitivity of tumors to photothermal therapy and chemotherapy drugs, are key issues that urgently need to be addressed in the current cancer treatment. In this work, polylactic acid-based drug nanoparticles (PLA@DOX/GA/ICG) were synthesized with good photothermal conversion ability by encapsulating the water-soluble anticancer drug doxorubicin (DOX), photothermal conversion agent indocyanine green (ICG) and liposoluble drug gambogic acid (GA) using a double emulsion method. The preparation process of PLA@DOX/GA/ICG was examined. Gambogic acid entrapped in PLA@DOX/GA/ICG nanoparticles could act as an HSP90 protein inhibitor to achieve bidirectional sensitization to chemotherapy and photothermal therapy under 808 nm laser irradiation for the first time, effectively ablating breast cancer cells *in vitro*. This nanodrug was expected to be used for the efficient treatment of tumors.

Open Access Article. Published on 05 July 2024. Downloaded on 1/18/2026 3:10:55 AM.
This article is licensed under a Creative Commons Attribution-NonCommercial 3.0 Unported Licence.

1 Introduction

Cancer is the second leading cause of death globally, with an increasing incidence due to the world's aging population.[1] The occurrence and development process of malignant tumor is a multi-stage complex process involving multiple factors and is regulated by multiple signaling pathways.[2–4] In the past, the clinical treatment effect on a single target was often not ideal.[5,6] The use of a specific target to achieve multi-point blockade of the malignant tumor signaling pathway network, thereby disrupting the entire signaling pathway network, has become a hot and complex topic in the medical field of cancer research.[7] The heat shock protein HSP90 plays an important role in numerous cell transduction pathways related to the occurrence, development, invasion, and metastasis of various malignant tumors.[8–10] Numerous studies worldwide have shown that the expression of HSP90 in malignant tumor tissues was 2–10 times higher than that in corresponding normal tissues.[11,12] HSP90 has a vast variety of client proteins, including Bcr/Ab1, ErbB2 (Her2), EGFR, Raf, Akt, MEK, and Src.[13–17] Among them, multiple customer proteins are protein kinases or transcription factors that play important roles in cell signal transduction pathways related to malignant tumor growth, invasion, and metastasis. By blocking the binding of HSP90 to client proteins, the biological activity of various client proteins related to the occurrence and development of malignant tumor could be lost, thus achieving the goal of "one target and multiple effects". Chemotherapy is the most commonly used method for cancer treatment. However, multidrug resistance to many chemotherapeutic molecules is easy to occur during the process of tumor chemotherapy, which limits its clinical application.[18–20] Photothermal therapy as an emerging strategy has gained increasing attention in cancer therapy recently.[21–27] NIR photothermal ablation could induce hyperthermia damage in cancer cells and tumor mass with deep tissue penetration. More importantly, the hyperthermia effect has been demonstrated to augment the cytotoxicity of some chemotherapeutic agents *in vitro* and *in vivo*, resulting in enhanced therapeutic efficacy for the treatment with low dosage of the drug. The combination of hyperthermia and chemotherapy has proven to be effective in optimizing the efficacy of some cancer cells.[28–32] However, under external stimuli such as drugs and photothermal therapy, tumor cells were always induced to produce heat shock protein HSP90 and increased the stress tolerance of the tumor to drugs and tumor ablation. Therefore, blocking the chaperone effect of HSP90 molecules was expected to improve the sensitivity of tumor chemotherapy, hyperthermia and other tumor ablation techniques.[25,33,34] In recent decades, researchers have successively applied HSP90 inhibitors for the prevention and treatment of prostate cancer, breast cancer, lung cancer, melanoma, chronic myeloid leukemia, multiple myeloma and other malignant tumors,[35–37] and many HSP90 inhibitors have also entered clinical trials.[38] Natural drugs have always been an

Henan Polytechinc University, Jiaozuo, Henan, 45400, China. E-mail: kongjichuan@hpu.edu.com; Wuchunhong@hpu.edu.com

† Electronic supplementary information (ESI) available. See DOI: https://doi.org/10.1039/d4ra01611d

© 2024 The Author(s). Published by the Royal Society of Chemistry

Open Access Article. Published on 05 July 2024. Downloaded on 1/18/2026 3:10:55 AM. This article is licensed under a Creative Commons Attribution-NonCommercial 3.0 Unported Licence.

important source of lead compounds discovered in the development of new antitumor drugs. Research has found that the natural product gambogic acid, as a novel HSP90 inhibitor, could bind to the C-terminal binding site of HSP90 and inhibit its binding to customer proteins.[39,40] It could effectively inhibit tumor cell proliferation *in vitro* and mouse-transplanted tumor models.[41] As a potential anticancer drug, it has been used in phase II clinical trials of non-small cell lung cancer, colon cancer and kidney cancer.[42] The FDA-approved angiographic agent indocyanine green (ICG) shows excellent photothermal conversion efficiency.[43,44] Nanosized drug delivery systems are considered a promising platform for cancer therapy as the nanoparticle delivery vehicles have unique abilities of enhanced permeation and retention effect (EPR) to overcome biological barriers, high loading efficiency, improved drug accumulation, targeted lesion sites, controlled drug release and prolonged pharmacological effects.[45–49] The preparation of biocompatible nanodrugs by co-loading doxorubicin[50] with ICG and GA could be expected to achieve bidirectional sensitization for chemotherapy and photothermal therapy, reducing the non-specific toxic side effects of doxorubicin and gambogic acid. The inhibitory effect of gambogic acid on the tumor predictive marker HSP90 could be used to achieve the treatment of "one target, multiple effects" on tumor. Therefore, we used FDA approved polylactic acid (PLA) as a carrier for pharmaceutical excipients, and co-encapsulates gambogic acid, doxorubicin and indocyanine green through a step-by-step emulsification method to prepare a multi-effect composite nanodrug, and investigated its combined ablation mechanism on tumor cells.

2 Materials and methods

2.1 Materials

All chemicals and reagents were used without further purification unless otherwise noted. Dulbecco's minimum essential medium (DMEM) cell culture medium, fetal bovine serum and trypsin were obtained from Gibco (USA), 4′,6-diamidino-2-phenylindole (DAPI) was purchased from Aladdin Reagent Co., Ltd (Shanghai, China). Thiazolyl blue (MTT) was obtained from Sigma-Aldrich (USA), dimethyl sulfoxide (DMSO) was obtained from Shanghai Biotech (China), polylactic acid (PLA) Poly-DL-active 0.70 dl g^{-1} were obtained from Shandong Medical Device Research Institute, polyvinyl alcohol (PVA, $[C_2H_4O]n$ 86–89%) were obtained from Alfa Aesar; Span-80 was obtained from Sigma-Aldrich (USA), ICG, GA and DOX were obtained from J&K Chemical Technology Company (Beijing, China), the experimental water was deionized water.

2.2 Preparation of nanomedicine

100 mg of PLA and 10 mg of GA were dissolved in 2 mL of dichloromethane as the organic phase. 10 mg of indocyanine green and 10 mg of doxorubicin hydrochloride were dissolved in 0.4 mL of deionized water as the aqueous phase. The aqueous phase was added dropwise to the organic phase followed by the addition of 3 drops of Span-80. Ultrasound dispersion was performed to form colostrum, then poured into a 2% PVA solution, further sonicated dispersion was performed and dichloromethane was evaporated by stirring. The precipitate after centrifugation was dispersed in deionized water, freeze-dried at low temperature, and stored at 4 °C for future use. The encapsulation efficiency (EE) and drug loading (LC) of the drug were calculated using the following formula:

$$\mathrm{LC} = \frac{W_0 - W_1}{W_2} \times 100\% \quad (1)$$

$$\mathrm{EE} = \frac{W_0 - W_1}{W_0} \times 100\% \quad (2)$$

W_0, W_1, and W_2 represent the initial DOX addition, the DOX content of the supernatant after centrifugation and the weight of the centrifuged precipitate after freeze drying, respectively.

2.3 Particle morphology characterization

The zeta potential and particle size distribution of multifunctional nanoparticles were measured using a dynamic light scattering laser particle size analyzer and zeta potential analyzer (He Ne laser light source: wavelength 632.8 nm). The method was used as follows: the prepared PLA@DOX/GA/ICG nanoparticle solution was sonicated in a water bath and diluted to a certain concentration, resulting in photon numbers ranging from 100 to 500 kcps during the sample testing process at room temperature of 25 °C.

The surface morphology of the multifunctional nanoparticles was characterized using the Quanta 200 FEG scanning electron microscope (accelerated voltage 20 kV) from FEI company in the United States. The method was as follows: a certain concentration of PLA@DOX/GA/ICG nanoparticles solution was prepared, and a micropipette was used to transfer a small amount of the sample solution that was dropped on a clean and flat silicon wafer, which was placed at 25 °C to dry, and gold was sprayed in vacuum for 2 minutes, followed by observations under a scanning electron microscope.

2.4 UV-vis spectroscopy

Scanning tests were conducted using a microplate reader at wavelengths between 400 and 900 nm to determine the absorption changes of the nanoparticle-loaded drugs from UV-vis spectra.

2.5 Photothermal performance

Different concentrations (0, 0.0625 mg mL^{-1}, 0.125 mg mL^{-1}, 0.25 mg mL^{-1}, 0.5 mg mL^{-1}, and 1.00 mg mL^{-1}) of NPs were deposited into quartz tubes and then subjected to an 808 nm continuous-wave laser at a power density of 1.0 W cm^{-2} for 5 min. A thermocouple probe with an accuracy of ±0.1 °C was inserted into the aqueous solution to measure the temperature change. The photothermal stability of NPs was also examined for 5 cycles. The photothermal conversion efficiency (η) was calculated using the following formula:

$$\eta = \frac{hS\Delta T_{\max} - Q_S}{I\left(1 - 10^{-A}\right)} = \frac{hS(\Delta T_{\max} - \Delta T_{\max s})}{I\left(1 - 10^{-A}\right)} \quad (3)$$

Open Access Article. Published on 05 July 2024. Downloaded on 1/18/2026 3:10:55 AM.
This article is licensed under a Creative Commons Attribution-NonCommercial 3.0 Unported Licence.

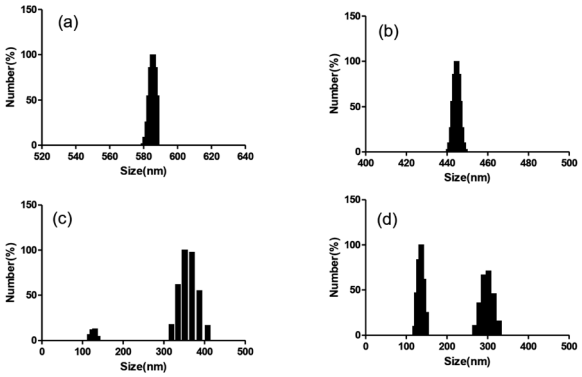

Fig. 1 Size distribution of PLA @DOX/GA/ICG nano-particles: (a) 0.5% PVA, ultrasonic dispersion for 30 s; (b) 1% PVA, ultrasonic dispersion for 30 s; (c) 1% PVA, ultrasonic dispersion for 3 min; (d) 2% PVA, ultrasonic dispersion for 3 min.

$$hS = \frac{m_s C_S}{\tau} \quad (4)$$

where ΔT_{max} represents the temperature change of the sample at the maximum steady-state temperature; ΔT_{maxs} represents the temperature change of the solvent at the maximum steady-state temperature; I is NIR laser power density; A represents the 808 nm absorbance of sample; C_s and m_s are the heat capacity and mass of solvent, respectively; τ is the sample system time constant, which can be determined by the linear curve fitting of temperature cooling time *vs.* its $\ln \frac{\Delta T}{\Delta T_{max}}$

2.6 *In vitro* stimuli-responsive release from the PLA@DOX/GA/ICG

PBS with different pH values (5.0 and 7.4) were selected as the release medium to study the pH-responsive release behavior of PLA@ DOX/GA/ICG. Briefly, 10 mL of PBS containing PLA@DOX/GA/ICG was added to a dialysis tube [molecular weight cut-off (MWCO) = 14 kD] immersed in 100 mL of release medium under gentle stirring at 37 °C or 45 °C. Release medium (2 mL) was collected at the given time intervals and 2 mL of fresh medium was added to the solution. The collected solution was used to measure the concentration of DOX using a UV-vis spectrophotometer at 480 nm.

2.7 *In vitro* cytotoxicity assays

The cytotoxicity was studied by MTT assay using 4T1 cells by taking the logarithmic growth stage cells and digesting them with trypsin to suspend them in the culture medium. The cells were seeded into a 96-well cell culture plate at 1×10^5 per well under 100% humidity and were cultured at 37 °C and 5% CO_2. After the cells adhered to the wall, they were cultured in media containing different final concentrations of the drugs. Each concentration was set with 6 wells and a blank control group (without cells, only the same volume of media was added) was also set. Cultivation was continued in an incubator at a temperature of 37 °C and a CO_2 concentration of 5% for 24 hours. MTT 100 μL was added to each well (concentration 0.5 mg mL^{-1}), further cultivating it in an incubator at 37 °C with a CO_2 concentration of 5% for 4 hours. The supernatant was carefully removed and 150 μL of DMSO was added per well. The mixer was shaken for 10 minutes and the light absorption value (*i.e.* OD value) was detected for each well

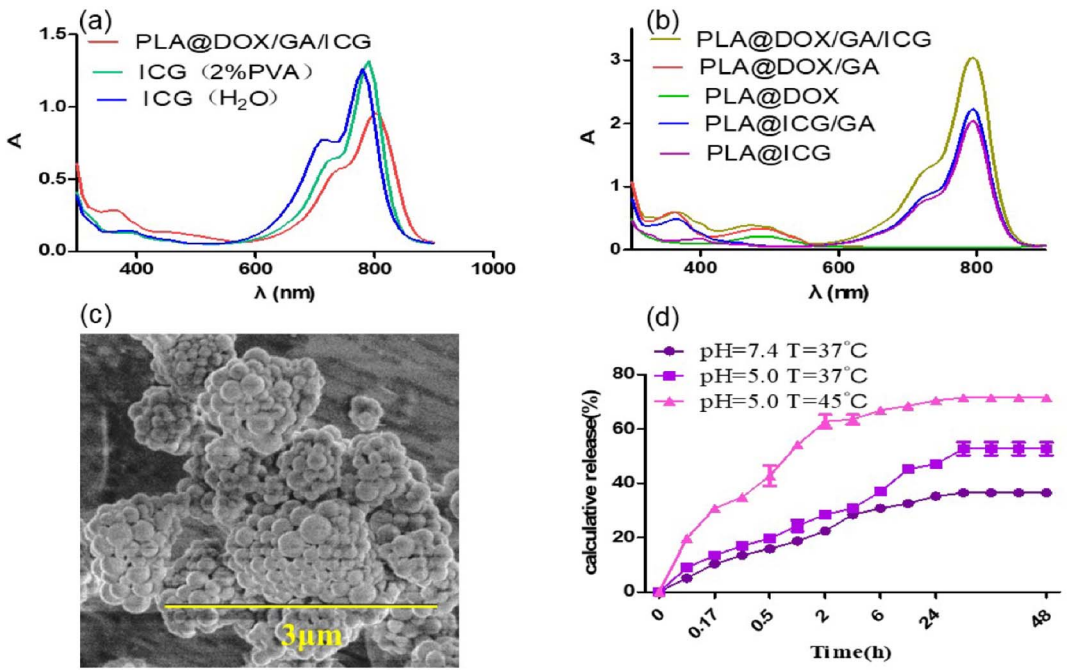

Fig. 2 (a and b) UV-vis absorption spectrum of medicine and nanoparticles; (c) SEM image of PLA@DOX/GA/ICG nanoparticles; (d) DOX release properties of nanodrugs.

© 2024 The Author(s). Published by the Royal Society of Chemistry

Open Access Article. Published on 05 July 2024. Downloaded on 1/18/2026 3:10:55 AM. This article is licensed under a Creative Commons Attribution-NonCommercial 3.0 Unported Licence.

cell at 570 nm using a Microplate reader. The cell survival rate was calculated using the following formula:

$$\text{The survival rate of the cell} = (\text{OD value of experimental group cell} - \text{OD value of blank control group})/(\text{OD value of control group cell} - \text{OD value of blank control group}) \times 100\%$$

2.8 Cellular uptake

Mouse breast cancer 4 T1 cells were cultured in normal DMEM culture medium with 10% FBS and 1% penicillin/streptomycin in 5% CO_2 and 95% air at 37 °C in a humidified incubator. The cellular uptake of PLA@DOX/GA/ICG nanodrugs was investigated using a fluorescence microscope. The tumor cells were seeded at a density of 1×10^5 cells per well into a 35 mm Petri dish and incubated at 37 °C for 12 h. Then, PLA@DOX/GA/ICG solutions were diluted to a final concentration of 100 μg mL^{-1} and cells were incubated for 3 h at 37 °C with DMEM as the control group. The cell monolayers were washed three times with phosphate-buffered saline (PBS, pH 7.4) and fixed with 4% paraformaldehyde for 30 min. Nucleus staining was performed with DAPI. After washing with PBS, cells were observed using a fluorescence microscope.

2.9 Apoptosis assay

4T1 cells in a 6-well plate were cultivated for 12 h, then PLA@Dox, PLA@Dox/GA, PLA@GA, PLA@ICG, PLA@GA/ICG 2 mL (content Dox 5 μg mL^{-1}, GA 5 μg mL^{-1}) were placed into the cell wells. After culturing for 4 h, the cells were irradiated with or without a NIR laser (1 W cm^{-2}) for 5 min and washed with PBS several times. AnnexinV-FITC and 7-AAD staining solution were added to the cell wells. They were then stained for 15 min under avoiding light. The apoptosis/necrosis status of the cells was then analyzed using flow cytometry.

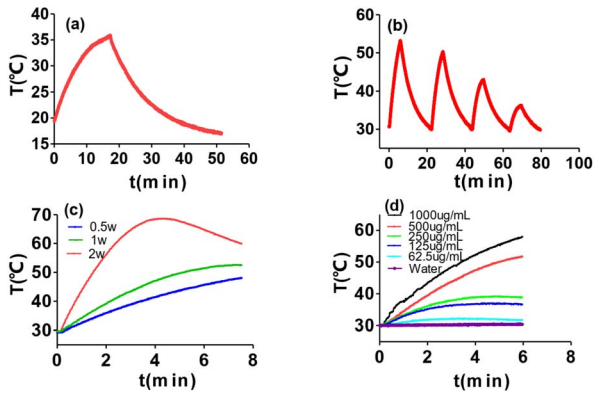

Fig. 3 Photothermal performance of PLA@DOX/GA/ICG; (a) and (b) real-time temperature measurement of PLA@DOX/GA/ICG suspensions (500 μg mL^{-1}, PLA@ DOX/GA/ICG1mL) under cycle laser irradiation (1 W cm^{-2}) for four cycles. Each cycle consisted of 5 min irradiation, followed by a cooling phase; (c) temperature elevation curves of PLA@DOX/GA/ICG suspensions at a concentration of 500 μg mL^{-1}, exposed to an 808 nm laser at various power densities; (d) temperature elevation curves of PLA@DOX/GA/ICG suspensions at various concentrations exposed to 1 W cm^{-2}.

2.10 Statistical analysis

The significance of experimental results was analyzed by a one-way variance (ANOVA) test and two-tailed Student's *t*-test using the Prism 5.0 software. Probabilities $p < 0.05$ (*), $p < 0.01$ (**), and $p < 0.001$ (***) were marked in each figure, and 0.05 was chosen as the significance level.

3 Results and discussion

3.1 Preparation and characterization of nanodrugs

Step-by-Step Emulsification Method ("W/O/W") was used to prepare drug loaded nanoparticles. The results indicated that both the ultrasonic dispersion time and the concentration of stabilizers attached had an impact on the particle size of nanoparticles. In 0.5% and 1% PVA solutions, 30% amplitude of the ultrasound dispersion was performed for 30 seconds, and dynamic light scattering was used to monitor the prepared nanoparticles with particle sizes of about 580 nm and 450 nm, Fig. 1a and b, respectively. This indicated that increasing the concentration of stabilizers could effectively increase the dispersion of nanoparticles and reduce their particle size distribution. Under the same conditions, extending the ultrasonic dispersion time to 3 minutes resulted in a reduction in the particle size of nanoparticles to approximately 300 nm and 130 nm (see Fig. 1c). However, as the concentration of the stabilizer increased and the ultrasound dispersion time prolonged, the encapsulation efficiency of the anticancer drug doxorubicin decreased from 91.4% to 70.1% (Table s1†). Considering the comprehensive factors, 2% PVA and ultrasonic dispersion for 3 minutes were used to prepare nanoparticles loaded drug (PLA@GA/DOX/ICG) for photothermal chemo-therapy. The UV-vis absorption curve showed characteristic absorption peaks of gambogic acid, doxorubicin and indocyanine green at 360 nm, 480 nm and 800 nm, respectively (see Fig. 2b), indicating that the prepared nanoparticles could achieve effectively drug encapsulation. The drug loading rates of gambogic acid, doxorubicin and indocyanine green were calculated using the standard curve method to be 5.81%, 4.51% and 5.01%, respectively. The UV visible absorption spectrum indicated that the increase in the maximum absorption redshift of indocyanine green encapsulated in nanoparticles was 20 nm, and shifted to 800 nm (see Fig. 2a), effectively overlapping the spectrum of the widely used 808 nm laser for photothermal effects,[51] which could further enhance the photothermal conversion efficiency. The particle size distribution investigated by dynamic light scattering was between 100–300 nm and these size particles could be engulfed by cells.[52] The scanning electron microscopy image showed that the drug-loaded nanoparticles were spherical and the particle size was consistent with the dynamic light scattering results (see Fig. 1d and 2c), but some aggregation was caused by the evaporation of the dispersed solvent. The zeta potential value of the PLA@GA/DOX/ICG aqueous dispersion system was −10.61 mV, indicating that the prepared drug-loaded nanoparticles could be stably dispersed in an aqueous medium.[53]

Open Access Article. Published on 05 July 2024. Downloaded on 1/18/2026 3:10:55 AM.
This article is licensed under a Creative Commons Attribution-NonCommercial 3.0 Unported Licence.

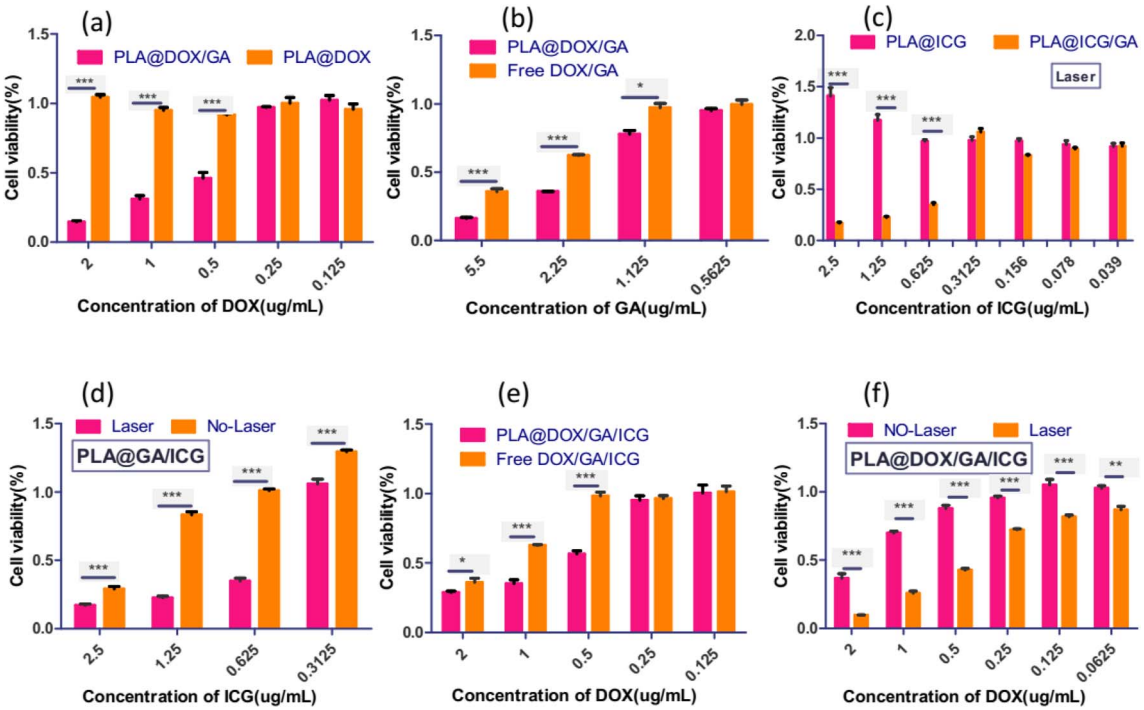

Fig. 4 Viability of 4T1 cells incubated with the nanoparticles or free DOX/GA/ICG at different concentrations with and without NIR irradiation at 1 W cm^{-2}. (a) Cell viability of 4T1 cells incubated with PLA@DOX and PLA@DOX/GA for 24 hours; (b) cell viability of 4T1 cells incubated with PLA@DOX/GA and free DOX/GA for 24 hours; (c) cell viability of 4T1 cells incubated with PLA@DOX/GA and free DOX/GA for 24 hours; (d) cell viability of 4T1 cells incubated with PLA@ICG/GA using laser or without laser treatment; (e) cell viability of 4T1 cells incubated with PLA@DOX/GA/ICG and free DOX/GA/ICG for 24 hours; (f) cell viability of 4T1 cells incubated with PLA@DOX/GA/ICG using laser or without laser treatment. Data are mean ± SD ($n = 5$, $^{*}p < 0.05$, $^{**}p < 0.01$, $^{***}p < 0.001$).

The drug release profiles of PLA@GA/DOX/ICG were assessed under the physiological (PBS, pH 7.4) and acidic conditions (PBS, pH 5.0) to simulate the endo-lysosomal environment at 37 °C and 45 °C. As shown in Fig. 2d, there was a much faster release of DOX at pH 5.0 solutions under 45 °C, thus achieving a high release content of 71%. The continuous release of PLA@GA/DOX/ICG occurred for more than seven days.

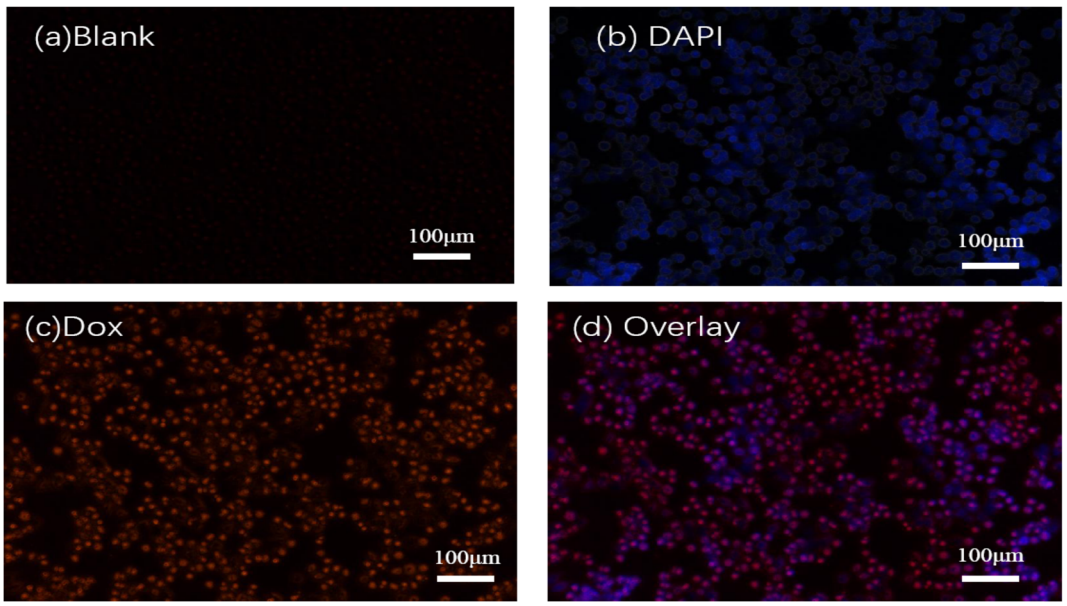

Fig. 5 Inverted fluorescence microscopy images of 4 T1 cells after the treatment with PLA@DOX/GA/ICG and DAPI. (a) Blank; (b) DAPI channel; (c)Dox channel; and (d) overlay.

© 2024 The Author(s). Published by the Royal Society of Chemistry

Open Access Article. Published on 05 July 2024. Downloaded on 1/18/2026 3:10:55 AM.
This article is licensed under a Creative Commons Attribution-NonCommercial 3.0 Unported Licence.

3.2 Photothermal conversion performance of nanomedicine

Under a laser with a wavelength of 808 nm and an optical density of 1w/cm^2, the temperature variation of PLA@DOX/GA/ICG with different concentrations differentiated with light exposure time. After 6 minutes of continuous irradiation, the temperature of the suspension (1 mL of 0.125 mg mL^{-1}) increased from 30 °C to 37 °C, as the concentration increased, the solution temperature continuously increased. When the concentration reached 1 mg mL^{-1}, the solution temperature increased to 61 °C, exceeding the tolerance temperature of cancer cells by 50 °C,[54] while the water temperature only increased by 1 °C (Fig. 3d). The photothermal conversion efficiency calculated from the single cycle photo-effect curve was 36.2% (Fig. 3a), which indicated that PLA@DOX/GA/ICG nanoparticles could be efficiently applied in photothermal therapy. Photothermal stability experiments were subjected by taking 0.5 mg mL^{-1} of the PLA@DOX/GA/ICG nanoparticle solution, it was found that the photothermal effect began to decrease due to the photobleaching effect of indocyanine green after repeating laser irradiation for 3 cycles[55] (Fig. 3b). The higher the optical density, the faster the temperature rise of the system, but the stronger the bleaching effect of light on nanodyes (Fig. 3c). Therefore, the selected illumination time for the subsequent experiment was 5 minutes and the optical density was 1 W cm^{-2}.

3.3 The effect of nanodrugs on tumor cells *in vitro*

To investigate the sensitization effect of gambogic acid on chemotherapy drugs and photothermal reagents, doxorubicin and indocyanine green were selected as models. PLA@DOX, PLA@DOX/GA, PLA@/ICG and PLA@ICG/GA were prepared according to the above procedure under the same conditions. When the concentration of doxorubicin of nanoparticles dispersion loaded with gambogic acid was 0.5 μg mL^{-1}, the survival rate of 4T1 cells decreased to 50% after cultured for 24 hours, while the cell activity of the nanoparticles without gambogic acid loading remained at nearly 100%. As the concentration increased, the cell activity gradually decreased to 18% (see Fig. 4a), indicating that gambogic acid could effectively enhance the killing effect of doxorubicin on tumor cells. Under the same conditions, the activity of cells incubating with PLA@DOX/GA nanoparticles was significantly lower than that of free DOX/GA mixed drugs (Fig. 4b), indicating that nanoparticles could more effectively increase the inhibitory effect of the drugs on cells.[56] PLA@ICG/GA nanoparticles with an indocyanine green concentration of 0.625 μg mL^{-1} were applied to the culture with 4T1 cells and incubated for 24 hours after treatment with 808 nm near-infrared light at a power density of 1 W cm^{-2} for 5 minutes. The survival rate of 4T1cells was about 40%, while the survival rate of cells without illumination remained above 90% (see Fig. 4d). Under the same conditions, PLA@/ICG nanoparticles were incubated with 4T1 breast cancer cells with the photothermal treatment, and the cell survival rate did not decrease (see Fig. 4c). The activity of the 4T1 cells incubated with PLA@ICG/GA was significantly reduced. Considering the cytotoxic effect of gambogic acid on cells, 4T1 cells were cultured with PLA@ICG/GA, followed by treatment with 1 W cm^{-2} near-infrared light. The results showed that as the concentration increased, the cell activity of the light-treated group decreased to 18%, which was lower than that of the control group cells without light treatment (see Fig. 4d). The above results indicated that gambogic acid could effectively sensitize photothermal therapy, reduce the thermal tolerance of tumor cells and achieve effective killing of tumor cells by hyperthermia.[57]

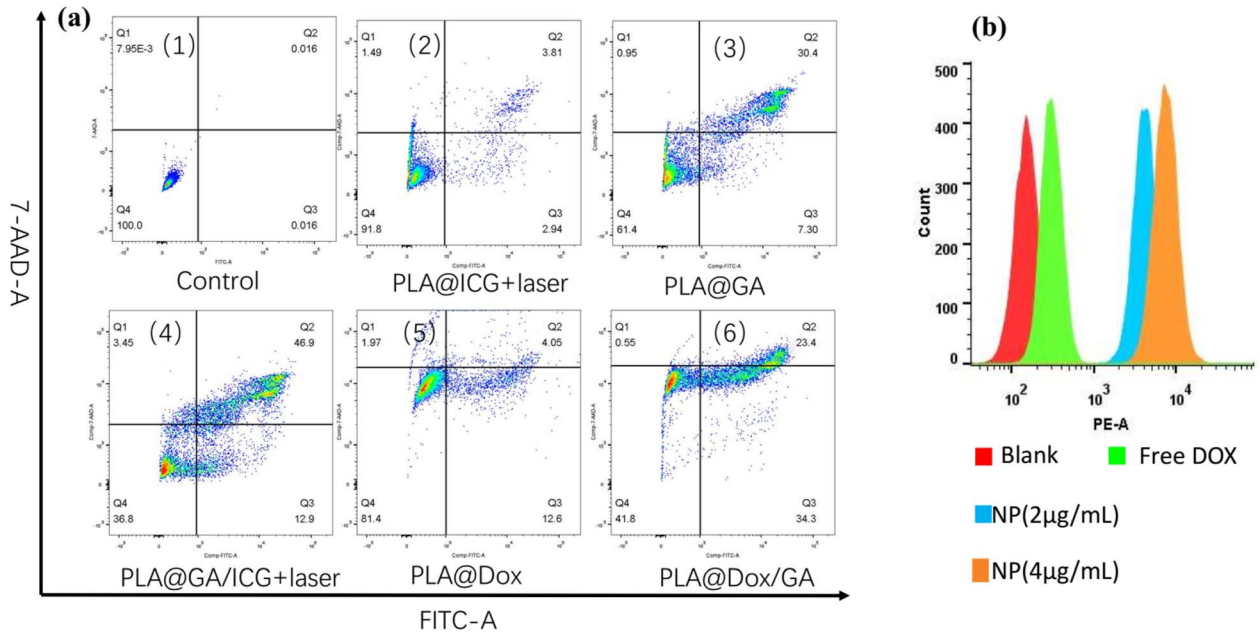

Fig. 6 (a) Flow cytometry analysis of 4T1 cell apoptosis induced by different nanoparticles with or without irradiation through Annexin V-FITC/7-AAD staining. (1) Control group; (2)PLA@ICG + laser; (3)PLA@GA; (4)PLA@GA/ICG + laser; (5)PLA@DOX; (6)PLA@DOX/GA. Bottom right quadrant: early apoptosis; top right quadrant: late apoptosis. (b) Flow cytometry for the investigation of cellular uptake to PLA@DOX/GA/ICG.

Open Access Article. Published on 05 July 2024. Downloaded on 1/18/2026 3:10:55 AM. This article is licensed under a Creative Commons Attribution-NonCommercial 3.0 Unported Licence.

PLA@DOX/GA/ICG nanoparticles with different concentrations were used to culture with 4T1 cells, the results are shown in Fig. 4. When the DOX content was 0.5 μg mL^{-1}, the cell survival rate was 59%, while the cell activity of the DOX/GA/ICG mixture group was above 95%, indicating that the nanoparticles had a stronger killing effect on 4TI cells due to the transport of nanoparticles (see Fig. 4e). When the concentration of DOX in the dispersion of PLA@DOX/GA/ICG nanoparticles was 0.5 μg mL^{-1}, the cell activity decreased to 42% after the light treatment at 808 nm. As the concentration increased, the cell survival rate decreased to 9.4%, significantly lower than that with the no-light treatment group (see Fig. 4f). Based on the above experimental results, it could be inferred that gambogic acid, as an HSP90 inhibitor, could inhibit the binding of HSP90 chaperone proteins to many customer proteins, and thereby increased the sensitivity of tumor cells to chemotherapy and photothermal therapy, achieving efficient chemotherapy combination photothermal therapy.[58,59]

3.4 Cellular uptake

The cellular uptake behaviors of PLA@DOX/GA/ICG in 4T1 cells were investigated by fluorescence microscope. As shown in Fig. 5c, red fluorescence was observed at the cytoplasm within the cells treated with PLA@DOX/GA/ICG for 3 h, while blue fluorescence in DAPI mode can be observed (Fig. 5b), the overlay single indicated that PLA@DOX/GA/ICG was taken up by the 4T1 cells (Fig. 5d). To further confirm the PLA@DOX/GA/ICG internalization in cells, 4T1 cells were incubated with free DOX and PLA@DOX/GA/ICG at different contents, then flowcytometry was carried out, the results are shown in Fig. 6b and they indicated that DOX can enter the 4T1cells, while PLA@DOX/GA/ICG could be more efficiently transported into cells to inhibit the cell growth by photothermal/chemotherapy.

3.5 *In vitro* antitumor mechanism

For the purpose of evaluating the *in vitro* antitumor mechanism of the nanoparticles against 4T1 cells, flow cytometry analysis was performed to investigate the 4 T1 cell apoptosis induced by various materials with irradiation. As shown in Fig. 6a, the PLA@ICG group exhibited no obvious cell apoptosis ratio in the presence of laser irradiation, PLA@GA exhibited a moderate cell apoptosis ratio of 37.7% (Fig. 6(1)). While the PLA@ICG/GA group after irradiation caused the most remarkable cell apoptosis, the cell apoptosis ratio reached 59.8%, indicating a result of the sensitization photothermal therapy of GA (Fig. 6(4)). The PLA@DOX group exhibited no obvious cell apoptosis ratio (Fig. 6(5)), as a result of the sensitization chemotherapy of GA, the apoptosis ratio of the PLA@DOX/GA group increased to 57.7% (Fig. 6(6)). The above results indicated that GA simultaneously increased cell sensitivity to the chemotherapy drugs and reduced cell heat resistance.

4 Conclusions

Reducing the tolerance of tumors to heat and the toxicity of chemotherapy drugs to the body, as well as increasing the sensitivity of tumors to photothermal therapy and chemotherapy drugs, are key issues that urgently need to be addressed in current cancer treatment. This study used a step-by-step emulsification method to prepare a three-component and dual-sensitized tumor cell ablation agent consisting of polylactic acid-loaded anticancer drug doxorubicin, photothermal reagent indocyanine green and chemotherapy photothermal sensitizer gambogic acid. The research results indicated that the nanoparticles not only had excellent photothermal conversion properties but also efficiently loaded the anticancer drugs doxorubicin and gambogic acid. While gambogic acid entrapped in PLA@DOX/GA/ICG nanoparticles could achieve bidirectional sensitization to chemotherapy and photothermal therapy under 808 nm laser irradiation for the first time, effectively ablating cancer cells with photothermal chemotherapy, this could also reduce the drug and thermal tolerance of tumor cells, effectively reducing the tumor cell ablation dose of the tumor drug doxorubicin. These are expected to be applied in the efficient ablation and photothermal chemotherapy synergistic treatment of solid tumors. As an HSP90 inhibitor, gambogic acid could inhibit its binding to many customer proteins, and does not affect the immune-related HSP70 function, it could be expected to achieve immunotherapy for distant metastatic tumors.[60]

Data availability

The data supporting this article have been included as part of the ESI.†

Conflicts of interest

There are no conflicts to declare.

Acknowledgements

This research was funded by the Fundamental Research Funds for the Universities of Henan Province grant number NSFRF220439 and Key scientific research projects of colleges and universities in Henan Province, grant number 23B350001.

References

1 I. Soerjomataram and F. Bray, *Nat. Rev. Clin. Oncol.*, 2021, **18**, 663–672.
2 Y. Zhang and X. Wang, *J. Hematol. Oncol.*, 2020, **13**, 165.
3 Y.-S. Jung and J.-I. Park, *Exp. Mol. Med.*, 2020, **52**, 183–191.
4 Y. Hisada and N. Mackman, *Blood*, 2017, **130**, 1499–1506.
5 F. Weiss, D. Lauffenburger and P. Friedl, *Nat. Rev. Cancer*, 2022, **22**, 157–173.
6 J. S. Lopez and U. Banerji, *Nat. Rev. Clin. Oncol.*, 2017, **14**, 57–66.
7 C. Braicu, M. Buse, C. Busuioc, R. Drula, D. Gulei, L. Raduly, A. Rusu, A. Irimie, A. G. Atanasov, O. Slaby, C. Ionescu and I. Berindan-Neagoe, *Cancers*, 2019, **11**, 1618.
8 S. Chatterjee and T. F. Burns, *Int. J. Mol. Sci.*, 2017, **18**, 1978.
9 J. Zhang, H. Li, Y. Liu, K. Zhao, S. Wei, E. T. Sugarman, L. Liu and G. Zhang, *Cells*, 2022, **11**, 2778.
10 M. P. Sumi and A. Ghosh, *Cells*, 2022, **11**, 976.

© 2024 The Author(s). Published by the Royal Society of Chemistry

Open Access Article. Published on 05 July 2024. Downloaded on 1/18/2026 3:10:55 AM. This article is licensed under a Creative Commons Attribution-NonCommercial 3.0 Unported Licence.

11 A. Zuehlke and J. L. Johnson, *Biopolymers*, 2010, **93**, 211–217.
12 H. Schwartz, B. Scroggins, A. Zuehlke, T. Kijima, K. Beebe, A. Mishra, L. Neckers and T. Prince, *Cell Stress & Chaperones*, 2015, **20**, 729–741.
13 J. Li, J. Soroka and J. Buchner, *Biochim. Biophys. Acta, Mol. Cell Res.*, 2012, **1823**, 624–635.
14 X. A. Lu, X. F. Wang, W. Zhuo, L. Jia, Y. S. Jiang, Y. Fu and Y. Z. Luo, *Biochem. J.*, 2014, **457**, 171–183.
15 D. Molenda, G. Kaemingk, P. Murphy, *FASEB Journal*, 2015, vol. 29.
16 J. M. Eckl and K. Richter, *Int. J. Biochem. Mol. Biol.*, 2013, **4**, 157–165.
17 W. B. Pratt, Y. Morishima, J. E. Gestwicki, A. P. Lieberman and Y. Osawa, *Exp. Biol. Med.*, 2014, **239**, 1405–1413.
18 S. Zeng, M. Poettler, B. Lan, R. Gruetzmann, C. Pilarsky and H. Yang, *Int. J. Mol. Sci.*, 2019, **20**, 4504.
19 Q. Wu, Z. Yang, Y. Nie, Y. Shi and D. Fan, *Cancer Lett.*, 2014, **347**, 159–166.
20 G. Housman, S. Byler, S. Heerboth, K. Lapinska, M. Longacre, N. Snyder and S. Sarkar, *Cancers*, 2014, **6**, 1769–1792.
21 D. Zhi, T. Yang, J. O'Hagan, S. Zhang and R. F. Donnelly, *J. Controlled Release*, 2020, **325**, 52–71.
22 L. Zhao, X. Zhang, X. Wang, X. Guan, W. Zhang and J. Ma, *J. Nanobiotechnol.*, 2021, **19**, 335.
23 J. Li, W. Zhang, W. Ji, J. Wang, N. Wang, W. Wu, Q. Wu, X. Hou, W. Hu and L. Li, *J. Mater. Chem. B*, 2021, **9**, 7909–7926.
24 H. S. Jung, P. Verwilst, A. Sharma, J. Shin, J. L. Sessler and J. S. Kim, *Chem. Soc. Rev.*, 2018, **47**, 2280–2297.
25 G. Gao, X. Sun and G. Liang, *Adv. Funct. Mater.*, 2021, **31**, 2100738.
26 N. Fernandes, C. F. Rodrigues, A. F. Moreira and I. J. Correia, *Biomater. Sci.*, 2020, **8**, 2990–3020.
27 N. S. Abadeer and C. J. Murphy, *J. Phys. Chem. C*, 2016, **120**, 4691–4716.
28 M. Zheng, C. Yue, Y. Ma, P. Gong, P. Zhao, C. Zheng, Z. Sheng, P. Zhang, Z. Wang and L. Cai, *ACS Nano*, 2013, **7**, 2056–2067.
29 Z. Zhang, J. Wang and C. Chen, *Adv. Mater.*, 2013, **25**, 3869–3880.
30 K. Yang, Y. Dong, X. Li, F. Wang and Y. Zhang, *Colloids Surf. B Biointerfaces*, 2023, **229**, 113437.
31 I. Psilopatis, C. Damaskos, N. Garmpis, K. Vrettou, A. Garmpi, P. Sarantis, E. Koustas, E. A. Antoniou, G. Kouraklis, A. Chionis, K. Kontzoglou and D. Dimitroulis, *Int. J. Mol. Sci.*, 2023, **24**, 12353.
32 P. Li, C. H. Liu, Y. Y. Zhao, D. D. Cao, B. Z. Chen, X. D. Guo and W. Zhang, *Biomacromolecules*, 2023, **24**, 3846–3857.
33 B. Tian, C. Wang, Y. Du, S. Dong, L. Feng, B. Liu, S. Liu, H. Ding, S. Gai, F. He and P. Yang, *Small*, 2022, **18**, e2200786.
34 J. Sun, Y. Li, Y. Teng, S. Wang, J. Guo and C. Wang, *Nanoscale*, 2020, **12**, 14775–14787.
35 C. V. Devarakonda, D. Kita, K. N. Phoenix and K. P. Claffey, *BMC Cancer*, 2015, **15**, 614.
36 J. Acquaviva, D. L. Smith, J.-P. Jimenez, C. Zhang, M. Sequeira, S. He, J. Sang, R. C. Bates and D. A. Proia, *Mol. Cancer Ther.*, 2014, **13**, 353–363.
37 K. L. Kaufman, Y. Jenkins, M. Alomari, M. Mirzaei, O. G. Best, D. Pascovici, S. Mactier, S. P. Mulligan, P. A. Haynes and R. I. Christopherson, *Oncotarget*, 2015, **6**, 40981–40997.
38 M. V. Powers and P. Workman, *FEBS Lett.*, 2007, **581**, 3758–3769.
39 K. H. Yim, T. L. Prince, S. Qu, F. Bai, P. A. Jennings, J. N. Onuchic, E. A. Theodorakis and L. Neckers, *Proc. Natl. Acad. Sci. U. S. A.*, 2016, **113**, E4801–E4809.
40 S. A. Fahmy, R. Elghanam, G. Rashid, R. A. Youness and N. K. Sedky, *RSC Adv.*, 2024, **14**, 4666–4691.
41 G. M. Huang, Y. Sun, X. Ge, X. Wan and C. B. Li, *World J. Gastroenterol.*, 2015, **21**, 6194–6205.
42 Y. Chi, X. K. Zhan, H. Yu, G. R. Xie, Z. Z. Wang, W. Xiao, Y. G. Wang, F. X. Xiong, J. F. Hu, L. Yang, C. X. Cui and J. W. Wang, *Chin. Med. J.*, 2013, **126**, 1642–1646.
43 D. Sheng, T. Liu, L. Deng, L. Zhang, X. Li, J. Xu, L. Hao, P. Li, H. Ran, H. Chen and Z. Wang, *Biomaterials*, 2018, **165**, 1–13.
44 Z. Y. Wang, Y. M. Ju, Z. Ali, H. Yin, F. G. Sheng, J. Lin, B. D. Wang and Y. L. Hou, *Nat. Commun.*, 2019, **10**, 12.
45 H. Zhao, J. Yu, R. Zhang, P. Chen, H. Jiang and W. Yu, *Eur. J. Med. Chem.*, 2023, **258**, 115612.
46 M. Xu, X. Han, H. Xiong, Y. Gao, B. Xu, G. Zhu and J. Li, *Molecules*, 2023, **28**, 5145.
47 D. Fan, Y. Cao, M. Cao, Y. Wang, Y. Cao and T. Gong, *Signal Transduct. Targeted Ther.*, 2023, **8**, 293.
48 J. Chandra, N. Hasan, N. Nasir, S. Wahab, P. V. Thanikachalam, A. Sahebkar, F. J. Ahmad and P. Kesharwani, *Environ. Res.*, 2023, **235**, 116649.
49 S. Batool, S. Sohail, F. U. Din, A. H. Alamri, A. S. Alqahtani, M. A. Alshahrani, M. A. Alshehri and H. G. Choi, *Drug Delivery*, 2023, **30**, 2183815.
50 Y. M. Ju, Z. Y. Wang, Z. S. Ali, H. C. Zhang, Y. Z. Wang, N. Xu, H. Yin, F. G. Sheng and Y. L. Hou, *Nano Res.*, 2022, **15**, 4274–4284.
51 S. Wu and H. J. Butt, *Adv. Mater.*, 2016, **28**, 1208–1226.
52 M. T. Zhu, G. J. Nie, H. Meng, T. Xia, A. Nel and Y. L. Zhao, *Acc. Chem. Res.*, 2013, **46**, 622–631.
53 B. Heurtault, P. Saulnier, B. Pech, J. E. Proust and J. P. Benoit, *Biomaterials*, 2003, **24**, 4283–4300.
54 L.-S. Lin, Z.-X. Cong, J.-B. Cao, K.-M. Ke, Q.-L. Peng, J. Gao, H.-H. Yang, G. Liu and X. Chen, *ACS Nano*, 2014, **8**, 3876–3883.
55 L. Lin, X. Liang, Y. Xu, Y. Yang, X. Li and Z. Dai, *Bioconjugate Chem.*, 2017, **28**, 2410–2419.
56 S. Gavas, S. Quazi and T. M. Karpinski, *Nanoscale Res. Lett.*, 2021, **16**, 173.
57 Y. Yang, W. Zhu, Z. Dong, Y. Chao, L. Xu, M. Chen and Z. Liu, *Adv. Mater.*, 2017, **29**, 1703588.
58 F. Sauvage, S. Messaoudi, E. Fattal, G. Barratt and J. Vergnaud-Gauduchon, *J. Controlled Release*, 2017, **248**, 133–143.
59 C. K. Dai, *Phil. Trans. Biol. Sci.*, 2018, **372**, 20160525.
60 J. Nam, S. Son, L. J. Ochyl, R. Kuai, A. Schwendeman and J. J. Moon, *Nat. Commun.*, 2018, **9**, 1074.